AIAA'85

AIAA-85-0074

The Design of Airfoils at Low Reynolds Numbers

M. S. Selig, Univ. of Illinois at Urbana-Champaign, Urbana, IL

AIAA 23rd Aerospace Sciences Meeting

January 14-17, 1985/Reno, Nevada

THE DESIGN OF AIRFOILS AT LOW REYNOLDS NUMBERS

Michael S. Selig*

University of Illinios at Urbana-Champaign

Abstract

This paper focuses on the design of airfoils at low Reynolds numbers (100,000<RN<500,000), specifically those applicable to radio-controlled model sailplanes. Two common types of airfoil lift and drag hysteresis are illustrated and explained in terms of the behavior of the upper-surface transitional separation bubble which is commonly present at these low Reynolds numbers. The theoretical section characteristics of several airfoils predicted by the Eppler computer program for the design and analysis of low-speed airfoils were compared with the recent experimental data of Althaus. Good correlation was found between the type of hysteresis and the general character of the pressure distribution. Also, the validity of the predicted section characteristics is discussed for this low Reynolds number regime. From the comparisons the desirable qualities of a low Reynolds number airfoil were determined. Based on this several airfoils for radio-controlled model sailplanes were subsequently designed and analyzed using the Eppler computer program.

Nomenclature

c	chord
C_ℓ	lift coefficient
C_d	drag coefficient
$C_{m_{c/4}}$	pitching-moment coefficient
RN	chord Reynolds number
v	local velocity
V_∞	free-stream velocity
V/V_∞	nondimensional velocity
x	airfoil abscissa
x/c	percent chord
α	angle of attack
α_0	angle of attack relative to the zero-lift line

Abbreviations

T.	boundary-layer transition
S.	boundary-layer separation
U.	airfoil upper surface
L.	airfoil lower surface

* Graduate Student, Department of Mechanical and Aerospace Engineering, Princeton University, Princeton, New Jersey
Student Member AIAA

I. Introduction

Increasing interest has been given to airfoils operating at chord Reynolds numbers (RNs) below 500,000. Radio-controlled (R/C) sailplanes, being the author's hobby and motivation for this study, fly in this RN regime. Additional applications include the following: remotely piloted vehicles at low speeds or high altitudes, inboard sections of helicopter rotor blades, human-powered aircraft, windmill blades, slats and flaps of high-lift, multi-element airfoils, struts on light aircraft, and turning vanes in air supply ducts.

This report focuses on the design of airfoils at low Reynolds numbers, specifically those applicable to R/C sailplanes. The approach taken in this study was to compare for several airfoils the theoretical section characteristics predicted by the Eppler computer program [1,2] with the experimental data of Althaus [3]. From these comparisons, the desirable qualities of a low RN airfoil were determined. Based on these comparisons, several R/C sailplane airfoils were designed and analyzed using the Eppler computer program.

II. Airfoils at Low Reynolds Numbers

For airfoils at low RNs, the phenomena of a transitional (or sometimes called laminar) separation bubble and turbulent separation significantly increase the drag and decrease the lift which both contribute to low lift-to-drag ratios. Increasing the RN will reduce the length of the transitional separation bubble and the extent of turbulent separation. Correspondingly, the lift-to-drag ratios increase. For the upper surface of the airfoil at positive angle of attack before stall, the boundary layer is laminar along the upper-forward surface of the airfoil. This laminar flow then separates upon entry into an adverse pressure gradient of sufficient magnitude and, quickly, undergoes transition to turbulent flow in the separated shear layer. Depending on the severity of the adverse pressure gradient following laminar separation, the separated turbulent boundary layer may or may not reattach to the surface of the airfoil. The region of recirculating air enclosed by the separation point and the reattachment point is the so-called transitional separation bubble. For the lower surface at positive angle of attack, the boundary layer is typically laminar and attached, though the possibility of separation does exist.

If the RN is low enough such that reattachment of the shear layer does not occur, increasing the RN to a value known as the critical RN causes reattachment. This RN may be identified by a dramatic increase in the lift-to-drag ratios and an approximately constant lift curve slope.

Hysteresis at Low Reynolds Numbers

As an airfoil is cycled through increasing angles of attack up to stall, the laminar separation point progresses forward. At some angle of attack, reattachment cannot occur, causing the transitional separation bubble to "burst." This bursting is manifested as a stall. For some airfoils cycled through decreasing angles of attack, the bubble does not behave in the same manner as it did for increasing angles of attack, thus accounting for the hysteresis shown in experimental lift, drag, and moment curves of these airfoils.

Two common types of airfoil lift hysteresis are found at low RN: (1) pre-stall hysteresis and (2) stall hysteresis shown in figures 1 and 2. In the case of pre-stall hysteresis, for increasing angle of attack a long transitional separation bubble, formed near the mid-chord, grows larger and may eventually extend into the wake. As this happens the lift curve begins to flatten out (a process which can be thought of as a trailing-edge stall) and the drag dramatically increases. Further increasing the angle of attack "unstalls" the airfoil by causing the long bubble to strangely collapse into a short bubble near the nose of the airfoil, resulting in markedly lower drag. Why the bubble collapses is not understood. Through decreasing angles of attack, a sharp decrease in lift occurs due to the reformation of the long bubble at an angle of attack lower than that at which the increase occurred. For some airfoils, the contraction and reformation of the long bubble happen at the same angle of attack, as for example several of the low RN Eppler airfoils [3]. Airfoils showing pre-stall hysteresis tend to have a high drag knee, that is, an increase in drag through the middle of the drag polar as a result of the bubble growing longer.

In contrast to pre-stall hysteresis caused by a long transitional separation bubble, stall hysteresis involves a short transitional separation bubble. In this case, before stall for increasing angle of attack, a short bubble exists on the leading edge of the airfoil. Further increasing the angle of attack causes the airfoil to stall either by the bursting of the bubble, a leading-edge stall, or by turbulent separation migrating towards the leading edge, a trailing-edge stall. Through decreasing angle of attack from stall, the short bubble reattaches, identified by a sharp increase in lift, at an angle of attack lower than that of stall for increasing angle of attack.

III. Influencing Transition

If it were possible for the boundary layer to make a transition before the laminar separation, the bubble and its drag and, if present, the hysteresis could all be eliminated. Several parameters which influence transition [4] are as follows:

1. boundary-layer suction and blowing
2. free-stream flow disturbances
3. surface roughness
4. pressure distribution (velocity distribution)

Although advantageous at low RNs, boundary-layer suction and blowing [5] are of little practical value to the modeler because of the complexity of such a suction or blowing device, and, for this reason, will not be discussed here. Also, disturbances in the free-stream flow will not be discussed as they are not applicable in the case of R/C sailplanes.

Surface roughness is a viable means of inducing transition at low RNs, though its use is minimal. It is a common practice for free flight modelers to place along the upper-forward portion of the airfoil surface a turbulator which when effectively positioned "artifically" causes transition before laminar separation, and thereby eliminates the bubble. The foremost disadvantage of the turbulator is its fixed position. While a turbulator may improve the overall performance of an airfoil at low RNs, at higher values the turbulator causes transition earlier than neccessary which results in more drag than there would otherwise be if it were moved aft as the RNs is increased. Therefore, one can understand why this method of influencing transition is employed mostly on free flight models that operate at very low RNs about which there are minimal fluctuations.

The influence of the pressure distribution on transition is discussed in a later section.

IV. Comparisons of Theoretical and Experimental Section Characteristics

The Eppler Computer Program

The theoretical section characteristics of several airfoils were computed using the Eppler computer program which has the following three primary capabilities: (1) potential flow design, (2) potential flow analysis, and (3) boundary-layer analysis. For the design method, the potential flow velocity distribution about an airfoil is specified. From this the airfoil coordinates are determined by conformal mapping. In the analysis method, the velocity distribution about a given airfoil is determined by a panel method.

To compute the section characteristics, the boundary-layer routines of the program incorporate an empirical transition criterion, and empirical skin friction, dissapation, and shape factor laws.

For RNs greater than those considered in this study, the theoretical section characteristics compare favorably with experimental measurements. As will be shown later, however, the program does not accurately predict the section characteristics of airfoils at low RNs since it makes the assumption that if the flow undergoes laminar separation before transition, the flow immediately reattaches as turbulent flow--the assumption of a short bubble. For higher RNs (1,000,000<RN<5,000,000), corresponding to those in the full-size sailplane regime, this quick reattachment is characteristics of the flow, but for lower RNs this assumption is not valid since the bubble can extend over most of the upper surface of the airfoil. If the program predicts a transitional separation bubble longer than three percent of the chord, it is noted in the output summary as a warning that the theoretical section characteristics may not be indicative of the actual section characteristics. As expected, this warning commonly appears for airfoils analyzed at low RNs.

The limitations of the program should be realized. Due to the incorporation of the short-bubble assumption, the present version of the program does not account for the additional bubble drag. If the program predicts turbulent separation, a small approximate drag penalty is added. Also, the program includes a correction for the pitching-moment and lift coefficients due to turbulent separation; however, it does not include a correction for the bubble. Despite this later exclusion, the theoretical maximum lift coefficient is in most cases indicative of the experimental maximum lift coefficient. With these limitations in mind, the theoretical section characteristics must be cautiously interpreted as discussed in further detail after the comparisons are made.

The Experimental Work of Althaus

Several problems are incountered in obtaining reliable experimental lift, drag, and moment measurements of an airfoil at low RNs. First, the ambient turbulence, tunnel noise, model vibration, and model surface contamination all force transition to occur earlier on the test model than in actual use. This has profound consequences--namely, it produces a shorter bubble and a hysteresis loop which is less pronounced than that found in actual use, which both combine to make the airfoil appear better than it actually is. Second, accurately measuring the extremely small lift, drag, and moment forces presents many difficulties. Because of these shortcomings, it is difficult to reliably conclude anything based on comparing data of airfoils tested in different wind tunnels.

In order that a self-consistent set of experimental data is considered, this paper will only compare data taken at a single facility. In part cular the author chose the data taken in 1980 by Althaus at the University of Stuttgart.

Comparisons

To study a broad range of behavior, eleven airfoils were chosen for comparison of the theoretical and experimental section characteristics. For this paper, however, only three airfoils, representative of the eleven, will be discussed. This is done without sacrifice to the clarity of this paper and the conclusions which follow. These three airfoils may be classified as follows:

1. GOE 801 --an airfoil with stall hysteresis without pre-stall hysteresis.
2. FX 61-140--an airfoil with pre-stall hysteresis without stall hysteresis.
3. FX 60-100--an airfoil with no hysteresis.

Excluded from this paper and discussed in reference 6 are the CLARK-Y, FX 63-137, E193, E392, GOE 795, NACA 0009, AH 79-100A, and MO6-13-128 [7].

For all airfoils compared, except those of Eppler, the original coordinates published in Althaus' book [3] had to be smoothed using a cubic spline smoothing program because the original coordinates caused irregularities in the velocity distribution to result as, for example, the FX 60-100 shown in figure 3. Since the boundary-layer routines of the Eppler computer program are highly sensitive to such irregularities, the theoretical section characteristics computed from the original coordinates are meaningless. The velocity distributions for the original and smoothed FX 60-100 are shown in figure 4. For most coordinates the difference between the original and smoothed coordinate was typically less than 0.0004c. In the case of wind tunnel models, it is probably true that these coordinates are similarly smoothed in the construction of the models.

To compare the theoretical and experimental drag polars, each airfoil was analyzed at the test RNs used by Althaus, and at a RN of 400,000. Analyzing each airfoil at a common RN of 400,000 permits the comparison of the theoretical data of one airfoil with another. In order to make comparisons of the lift vs. drag data, Althaus' experimental data is co-plotted with the theoretical data. Commonly, due to a high drag knee at the lower test RNs of Althaus, only a few experimental data points could be co-

plotted at the high- and low-lift ends of the drag polar. In these cases only those data points at the low-lift end were co-plotted. Also, Althaus' experimental lift curves are shown to illustrate the lift hysteresis. Co-plotted on these lift curves is the theoretical lift curve to show discrepencies which will be discussed.

The airfoil velocity distributions were plotted for angles of attack relative to the zero-lift line in increments of one or two degrees. The increment that was use can be distinguished by the relative differences in spacing between two adjacent velocity distributions.

The Theoretical Boundary-Layer Summary Table shown with each airfoil should be used as a guide to evaluating the theoretical section characteristics. When a "*" appears it indicates that the program predicts a transitional separation bubble longer than 0.03c. For these cases the predicted drag is most likely too low since the program does not account for the additional bubble drag. When a "O" appears it indicates that the bubble if present at all is shorter than 0.03c. In these cases agreement between the theoretical and experimental drag should be expected. If the predicted bubble is shorter than 0.03c and transition occurs before 0.05c, a "●" indicates this. Agreement for these cases is generally good. When a "-" appears it indicates separation without reattachment--a stall. The symbol "+" has been placed beside the angles of attack relative to the zero-lift line which are within the low-drag range of the drag polar.

It was observed that airfoils with pre-stall hysteresis, for example the FX 61-140 shown in figures 5-8, have a concave potential flow velocity recovery region on the upper surface, and airfoils without pre-stall hysteresis have a convex to linear velocity recovery, for instance the GOE 801 and FX 60-100 shown in figures 9-12 and 13-16. With the concave recovery the flow separates upon entry into the adverse pressure gradient of the recovery. Since the gradient is steep, reattachment does not occur immediately, forming a long bubble. When the angle of attack is increased, the pressure gradients become steeper. As a consequence of this, reattachment takes place futher downstream, the bubble then grows longer, and the drag increases until the bubble collaspes to the nose as discussed in the section on hysteresis. With a convex recovery having gradients not as steep as those of a concave recovery, the flow separates and reattaches rather easily. For increasing angles of attack the separation point and reattachment point both move forward toward the leading edge with the reattachment point moving forward at a slightly greater rate such that the bubble decreases in length. The bubble then does not collapse causing pre-stall hysteresis.

Stall hysteresis appears to be caused by pressure gradients on the upper surface of the airfoil which are less severe, in the range of stall, than the gradients of airfoils without stall hysteresis. To illustrate this, compare the upper-forward surface velocity distribution, denoted by a small arrow, of the GOE 801, FX 61-140, and FX 60-100 at an angle of attack of 12 degrees relative to the zero-lift line. It is seen that the gradients of the GOE 801 having stall hysteresis are less relative to the FX 61-140 and FX 60-100 both having no stall hysteresis. There may be a tendency to conclude from the presented examples that a large nose radius yields pressure gradients conducive to causing stall hysteresis. While this conclusion may in part be correct, it is more judicious to believe that the stall hysteresis or lack thereof is caused by the entire upper forward surface pressure distribution and not singly the pressure distribution in the vicinity of the nose

It was found that the larger the difference between the upper-surface and lower-surface nondimensional velocity just before the trailing edge, called here the trailing edge velocity differential, the poorer the agreement between the predicted and experimental lift. The FX 61-140 with a large trailing edge velocity differential is an example of such poor agreement. This may be explained by considering the steep pressure gradients on the upper surface at the trailing edge. The steep gradients here likely lead to turbulent separation on the upper surface that extends further upstream than can be predicted by conventional boundary-layer methods. For the GOE 801 the velocity differential is not as large as the FX 61-140, and the agreement in lift is much better. The FX 60-100 is an intermediate case.

As discussed in reference 8, if no transitional separation bubble is predicted on the upper surface, the agreement between the theory and experiment is often better than when a bubble is predicted. This fact suggests that the bubble predict criterion is valid. Due to the limited number of comparisons made in this paper, it is not possible here to illustrate this point by means of examples.

It is imaginable that there exists an airfoil with a concave recovery, similar to that of the FX 61-140, and gradual pressure gradients near the upper surface leading edge, similar to those of the GOE 801. From the preceeding discussion regarding the relationship between the general character of the pressure gradients and the exhibited hysteresis, this hypothesized airfoil would be expected to have both pre-stall and stall hysteresis [8]. Whether this is the case remains to be seen.

V. R/C Sailplane Airfoil Design Considerations

In designing airfoils for use on R/C sailplanes, stall hysteresis of the airfoil is permissible if it takes place, as it typically does, at angles of attack outside of the usual flight regime. An airfoil with pre-stall hysteresis, however, should be avoided on account of the low lift-to-drag ratios attained, due to the high drag knee, through the mid-range of the drag polar. Another deterent to using an airfoil with pre-stall hysteresis is the fact that the airfoil lift coefficient tends to "bounce" up and down if operated within the hysteresis loop. This naturally leads to pitch oscillations of the sailplane, making smooth flight literally impossible. Of course, if the hysteresis loop is not too large, this effect is secondary to the devistating effects of the high drag knee.

For R/C sailplanes in steady, level flight, the flight speed, and therefore the RN, varies inversely as the square root of the aircraft lift coefficient. To an advantage this fact may be used. At low RNs corresponding to high lift coefficients it is desirable to have the flow transition early after laminar separation allowing for quick reattachment, thereby avoiding the drag of a long transitional separation bubble. Whereas at high RNs corresponding to low lift coefficients, later transition (more laminar flow) followed by quick reattachment is possible, which permits a lower drag. As discussed a turbulator effectively achieves this quick transition and reattachment at low RNs, but it results in a greater drag than necessary at high RNs. By the design of the upper forward surface velocity distribution, transition may be made to occur early (5-15% c) at low RNs, high lift coefficients, and late (45-55% c) at high RNs, low lift coefficients. When this is done, a transitional separation bubble is predicted less frequently and the theoretical drag slowly increases with increasing angle-of-attack rather than a theoretical drag which suddenly increases near stall as, for example, in the case of the FX 61-140.

Based on these considerations, several airfoils have been designed by the author for use on R/C sailplanes [9], though not exclusively for this application. The S2091-101-83 shown in figures 17-19 is one such example. It is based on the AQUILA airfoil [8] which by way of its flat lower surface suffers from poor wind penetration owing to high drag caused by lower surface flow separation at low angles of attack. The S2091-101-83 has an extended low-lift, low-drag range, which allows for better penetration without compromising the high-lift capabilty of the AQUILA airfoil. This new airfoil has a convex recovery to prevent pre-stall hysteresis. The prediction of the lift is expected to be good since no large velocity differential exists at the trailing edge. As indicated by the Theoretical Boundary-Layer Summary Table, the drag of this airfoil should be as predicted by theory. In studying the velocity distribution of the upper forward surface, stall hysteresis may be present. Coordinates for this airfoil are given in figure 20.

VI. Concluding Remarks

In designing airfoils for low RNs, a convex recovery is favored over a concave recovery, thus preventing pre-stall hysteresis and its associated lift and drag penalties. Large velocity differentials near the trailing edge which result in steep adverse pressure gradients should be avoided, and the transition point should be designed to move forward toward the leading edge with increasing angles of attack in order to minimize the areas of laminar and turbulent separation that are detrimental to the performance of an airfoil. Some new airfoils have been designed with these considerations and should prove to be successful in application to R/C sailplanes. To use the Eppler computer program for the design and analysis of low RN airfoils, the limitations of the boundary-layer analysis, as discussed, must be considered when designing and choosing an airfoil for use in the R/C sailplane regime.

VII. Acknowledgements

The author expresses special thanks to Dr. Mark D. Maughmer, Professor of Aerospace Engineering at Pennsylvania State University, for making available the Eppler computer program. In addition, the author especially thanks him for their many discussions throughout the course of this work.

VIII. References

1. Eppler, Richard and Somers, Dan M., "A Computer Program for the Design and Analysis of Low-Speed Airfoils," NASA TM-80210, August, 1980.
2. Eppler, Richard and Somers, Dan M., "Low Speed Airfoil Design and Analysis," Proceedings of the NASA Advanced Technology Airfoil Research Conference NASA CP-2045, Part 1, March 1978.
3. Althaus, Dieter, Profilpolaren Fur Den Modellflug,Villingen-Schwennigen: Necker-Verlag, 1980.
4. Schlicting, Herman, Boundary-Layer Theory, 7th ed. Trans. by J. Kestin, New York: McGraw-Hill, 1979.
5. Horstmann, K. H. and Quast, A., "Reduction of Section Drag by Blowing Through Holes in Areas of Laminar Separation Bubbles,"Technical Soaring," Vol. VII, No. 1, September 1981.
6. Selig, Michael S., "The Design of Airfoils at Low Reynolds Numbers," Paper presented at the AIAA 1984 Student Paper Conference held at Purdue University on March 23-24, 1984.

7. Mueller, T. J. and Pohlen, L. J., "Boundary Layer Characteristics of the Miley Airfoil at Low Reynolds Numbers," AIAA-83-1795, July 1983.
8. Selig, Michael S., "Addendum to the Design of Airfoils at Low Reynolds Numbers," SOARTECH IV, c/o H. A. Stokely, 1504 Horseshoe Circle, Virginia Beach, Virginia, 23451, January 1985.
9. Selig, Michael S., "The Design of Airfoils at Low Reynolds Numbers," SOARTECH III, c/o H. A. Stokely, 1504 Horseshoe Circle, Virginia Beach, Virginia, 23451, July 1984.

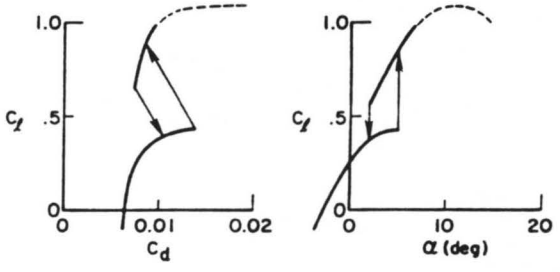

Fig. 1 Performance of an airfoil with pre-stall hysteresis.

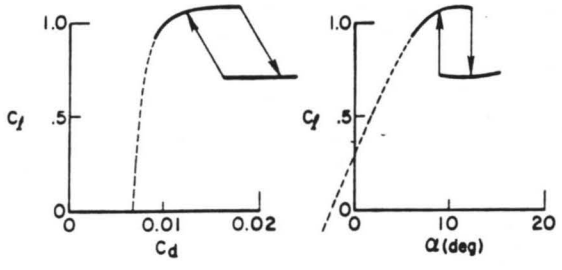

Fig. 2 Performance of an airfoil with stall hysteresis.

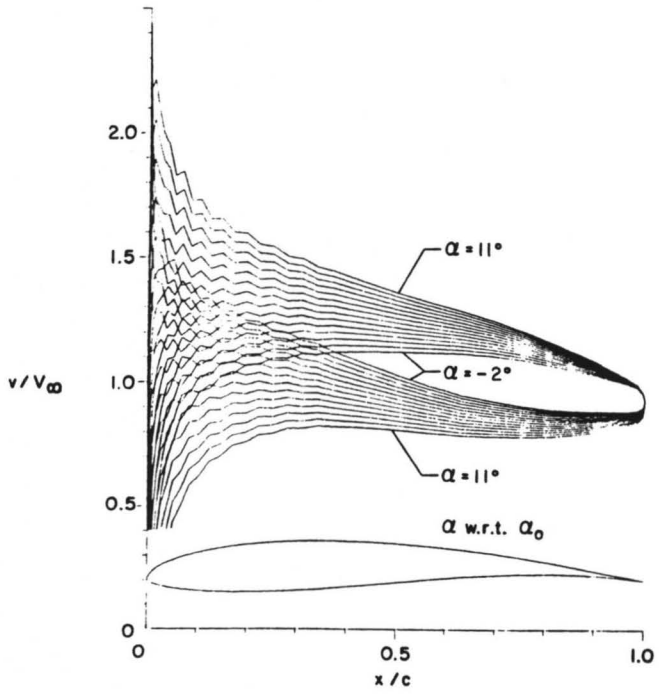

Fig. 3 Velocity distribution of the FX 60-100 based on the original coordinates.

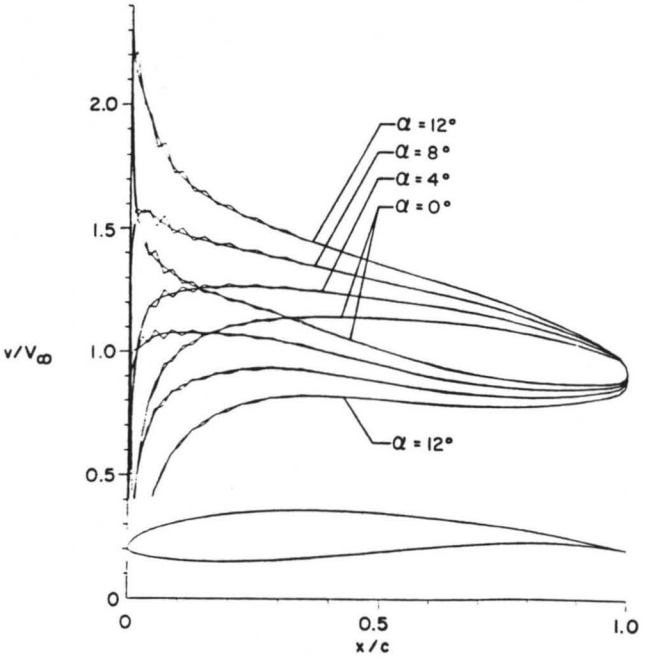

Fig. 4 Comparison of the velocity distributions for the original and smoothed coordinates for the FX 60-100.

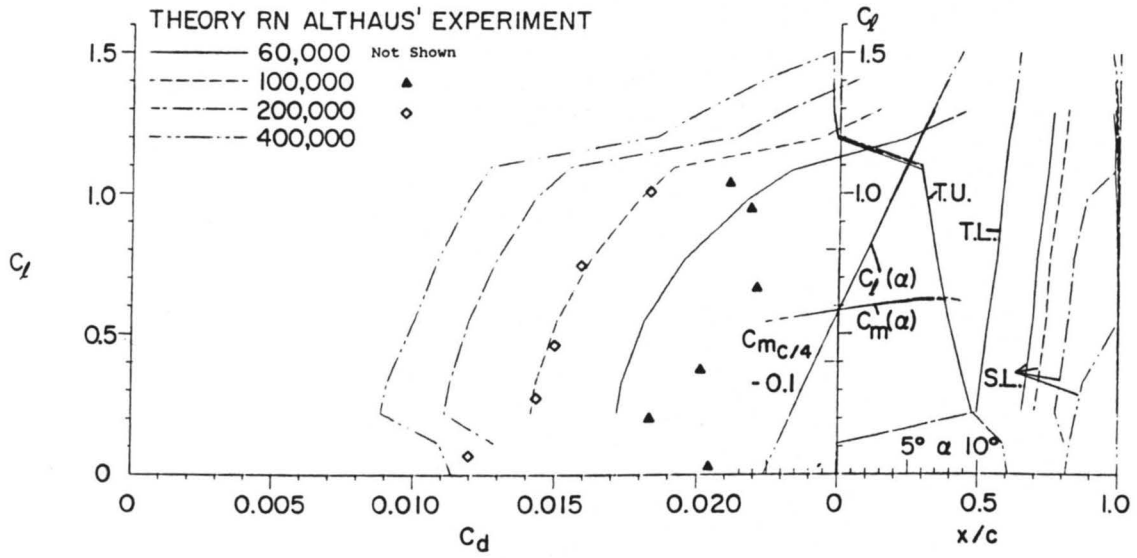

Fig. 5 Comparison of the theoretical and experimental section characteristics for the FX 61-140.

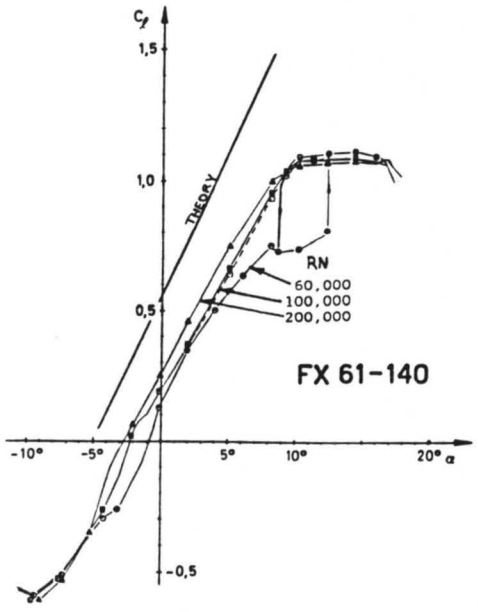

Fig. 6 Comparison of the theoretical and experimental lift curves for the FX 61-140.

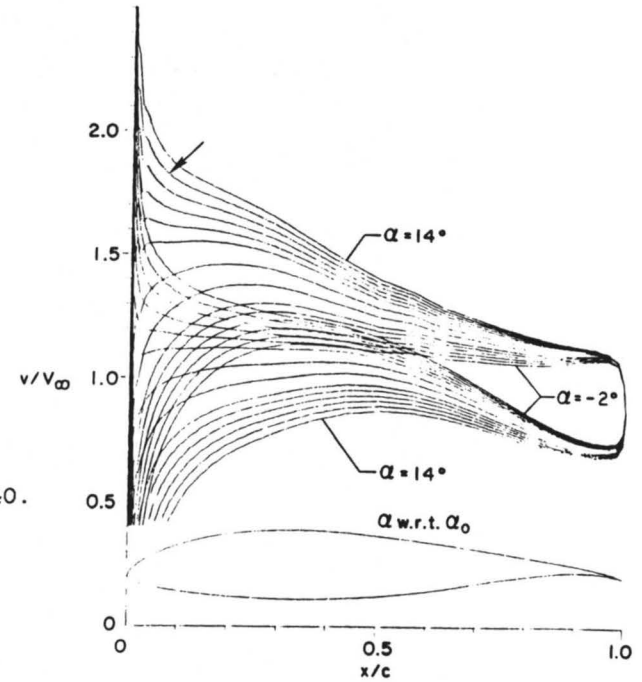

Fig. 8 Velocity distributions for the FX 61-140.

THEORETICAL BOUNDARY-LAYER SUMMARY TABLE

AIRFOIL: FX 61-140

*-LAMINAR SEPARATION BUBBLE WARNING
O-NO SEPARATION BUBBLE WARNING
●-NO BUBBLE, TRANSITION BEFORE 0.05C
--SEPARATION AT LEADING EDGE (STALL)
←-ANGLE OF ATTACK WITHIN DRAG BUCKET

ALPHA (deg)	REYNOLDS NUMBER 60000 us	60000 ls	100000 us	100000 ls	200000 us	200000 ls	400000 us	400000 ls	us	ls
0	-	-	-	-	-	-	●	●		
1	-	-	-	-	●	●	●	●		
+ 2	●	●	●	●	●	●	●	●		
+ 3	●	●	●	●	●	●	●	●		
+ 5	●	●	●	●	●	●	●	●		
+ 7	●	●	●	●	●	●	●	●		
+ 9	●	●	●	●	●	●	●	●		
+10	●	●	●	●	●	●	●	●		
11	●	●	●	●	●	●	●	●		
12	●	●	●	●	●	●	●	●		
13	●	●	●	●	●	●	●	●		
14	●	●	●	●	●	●	●	●		

Fig. 7 FX 61-140 Theoretical Boundary-Layer Summary Table.

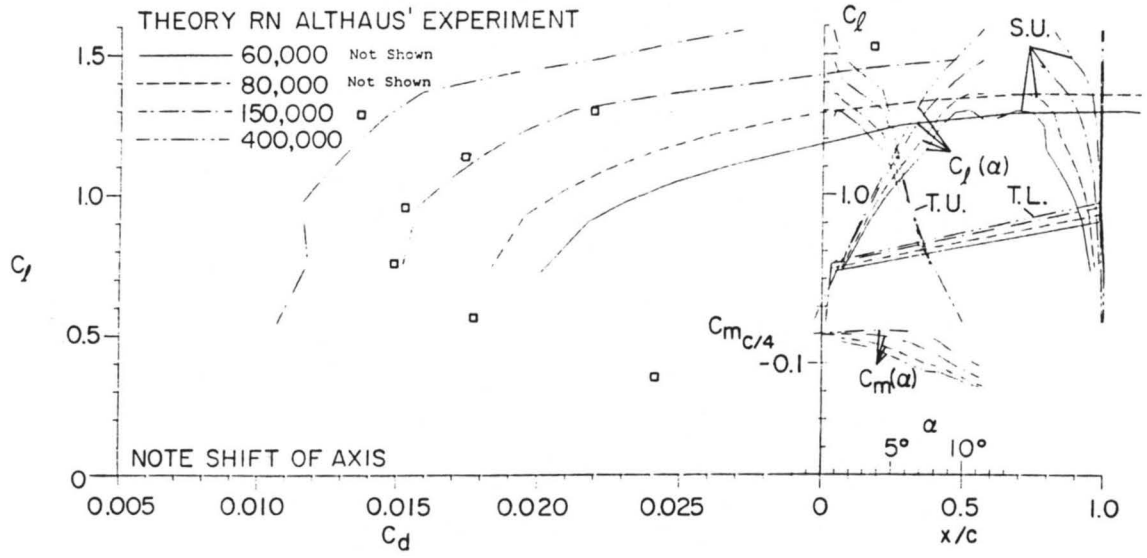

Fig. 9 Comparison of the theoretical and experimental section characteristics for the GOE 801.

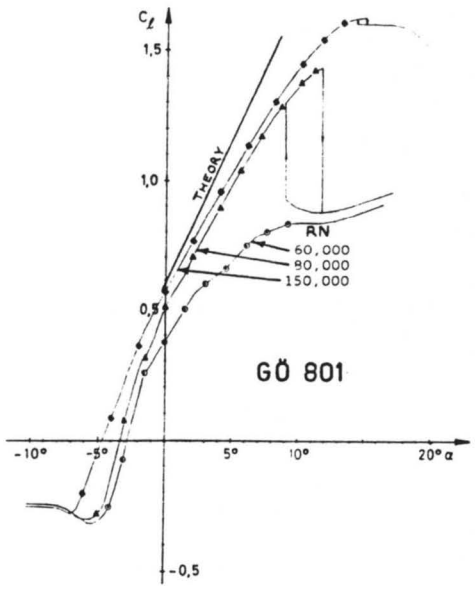

Fig. 10 Comparison of the theoretical and experimental lift curves for the GOE 801.

THEORETICAL BOUNDARY-LAYER SUMMARY TABLE										
AIRFOIL	*-LAMINAR SEPARATION BUBBLE WARNING 0-NO SEPARATION BUBBLE WARNING ●-NO BUBBLE, TRANSITION BEFORE 0.05C --SEPARATION AT LEADING EDGE (STALL)									
GOE 801	+-ANGLE OF ATTACK WITHIN DRAG BUCKET									
ALPHA (deg)	REYNOLDS NUMBER									
	60000		80000		150000		400000			
	us	ls	us	ls	us	ls	us	ls	us	ls
5	-	-	-	-	-	-	●	●		
7	●	●	●	●	●	●	●	●		
+ 9	●	●	●	●	●	●	0	●		
+10	●	●	●	●	●	●	0	●		
+11	●	●	●	●	●	●	0	●		
+12	●	●	●	●	●	●	0	●		
+13	●	●	●	●	●	●	0	●		
+14	●	●	●	●	●	●	0	●		
+15	●	●	●	●	0	●	0	●		
16	●	●	●	●	●	●	●	●		
17	●	●	●	●	●	●	●	●		

Fig. 11 GOE 801 Theoretical Boundary-Layer Summary Table.

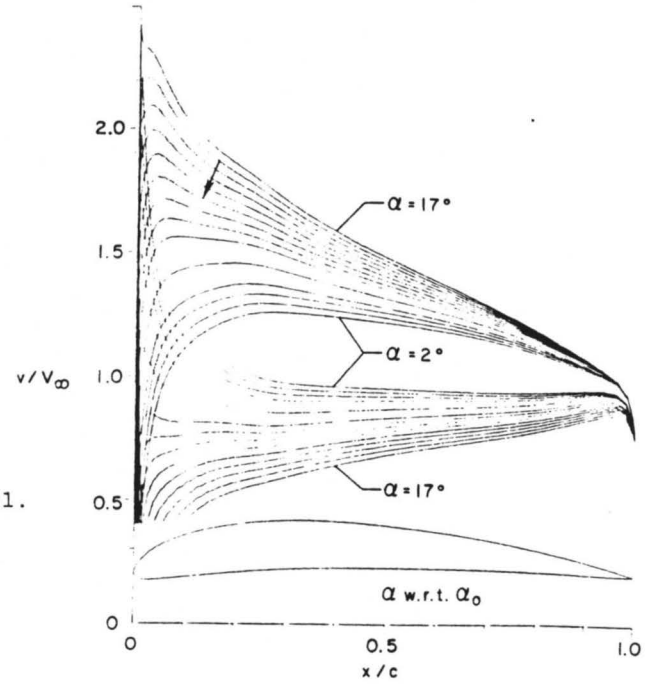

Fig. 12 Velocity distributions for the GOE 801.

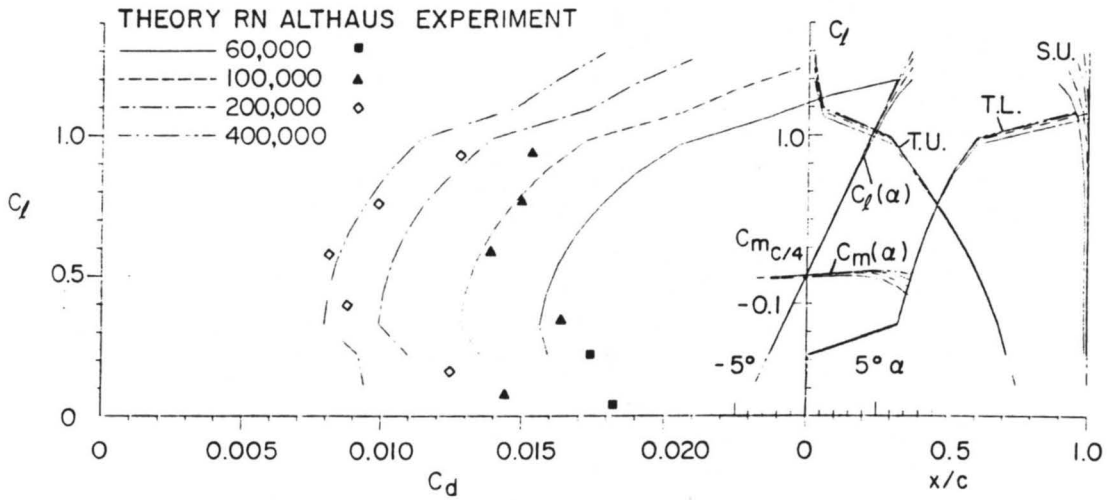

Fig. 13 Comparison of the theoretical and experimental section characteristics for the FX 60-100.

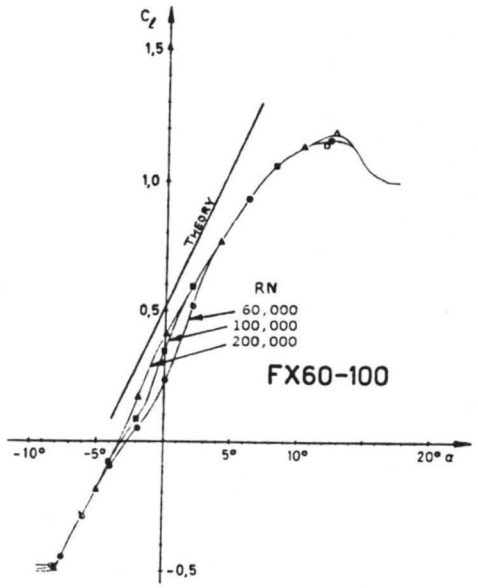

Fig. 14 Comparison of the theoretical and experimental lift curves for the FX 60-100

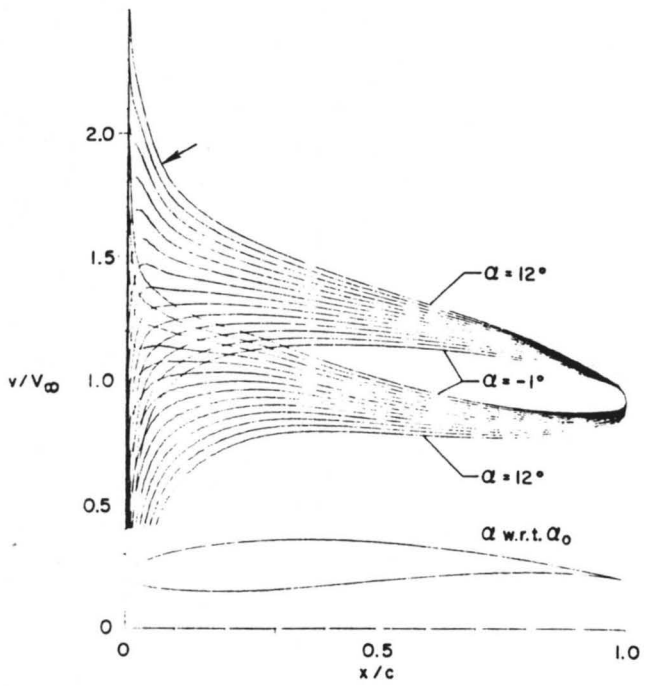

Fig. 16 Velocity distributions for the FX 60-100.

THEORETICAL BOUNDARY-LAYER SUMMARY TABLE

AIRFOIL
*-LAMINAR SEPARATION BUBBLE WARNING
O-NO SEPARATION BUBBLE WARNING
●-NO BUBBLE, TRANSITION BEFORE 0.05C
--SEPARATION AT LEADING EDGE (STALL)
FX 60-100
+-ANGLE OF ATTACK WITHIN DRAG BUCKET

ALPHA (deg)	REYNOLDS NUMBER 60000 us	ls	100000 us	ls	200000 us	ls	400000 us	ls	us	ls
1	-	-	-	-	-	-	●	●		
2	●	●	●	●	●	●	●	●		
+ 3	●	●	●	●	●	●	●	●		
+ 4	●	●	●	●	●	●	●	●		
+ 5	●	●	●	●	●	●	●	●		
+ 6	●	●	●	●	●	●	●	●		
+ 7	●	●	●	●	●	●	●	●		
+ 8	●	●	●	●	●	●	●	●		
+ 9	●	●	●	●	●	●	●	●		
+10	●	O	●	O	O	O	O	O		
11	●	O	●	O	●	O	●	O		
12	●	O	●	O	●	O	●	O		

Fig. 15 FX 60-100 Theoretical Boundary-Layer Summary Table.

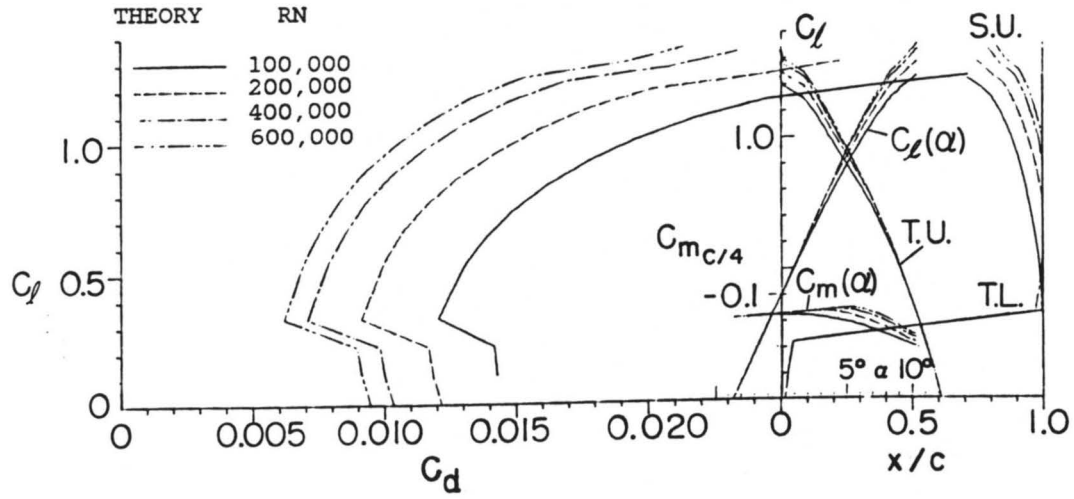

Fig. 17 Theoretical section characteristics for the S2091-101-83.

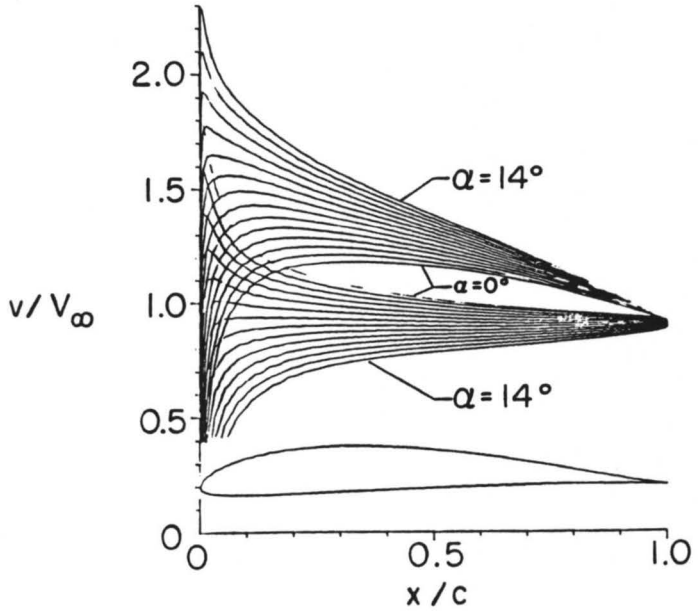

Fig. 18 Velocity distributions for the S2091-101-83.

THEORETICAL BOUNDARY-LAYER SUMMARY TABLE										
AIRFOIL	*-LAMINAR SEPARATION BUBBLE WARNING									
	O-NO SEPARATION BUBBLE WARNING									
	●-NO BUBBLE, TRANSITION BEFORE 0.05C									
	--SEPARATION AT LEADING EDGE (STALL)									
2091-101-83	+-ANGLE OF ATTACK WITHIN DRAG BUCKET									
ALPHA (deg)	REYNOLDS NUMBER									
			100000		200000		400000		600000	
	us	ls	us	ls	us	ls	us	ls	us	ls
0			*	*	*	*	*	●	*	●
1			*	*	*	*	*	●	*	●
+ 2			*	*	*	●	*	●	*	●
+ 3			*	*	*	*	*	*	*	*
+ 5			*	O	*	O	*	O	*	O
+ 6			*	O	*	O	*	O	O	O
+ 7			*	O	*	O	*	O	O	O
+ 8			*	O	*	O	*	O	O	O
+ 9			*	O	*	O	O	O	O	O
+10			*	O	*	O	O	O	O	O
+11			*	O	*	O	O	O	O	O
+12			*	O	O	O	O	O	O	O
13			●	O	●	O	●	O	●	O
14			*	O	●	O	●	O	●	O

Fig. 19 S2091-101-83 Theoretical Boundary-Layer Summary Table.

X	Y
1.00000	0.00000
.99674	.00035
.98707	.00150
.97126	.00367
.94970	.00699
.92292	.01150
.89147	.01713
.85594	.02373
.81693	.03107
.77501	.03888
.73070	.04689
.68454	.05479
.63700	.06231
.58856	.06920
.53965	.07526
.49073	.08029
.44220	.08416
.39450	.08677
.34805	.08805
.30323	.08794
.26043	.08644
.22002	.08356
.18232	.07934
.14765	.07382
.11622	.06708
.08823	.05927
.06384	.05060
.04320	.04130
.02645	.03168
.01374	.02205
.00517	.01269
.00077	.00401
.00058	-.00312
.00575	-.00864
.01662	-.01315
.03263	-.01645
.05397	-.01844
.08063	-.01936
.11236	-.01939
.14883	-.01873
.18960	-.01750
.23417	-.01581
.28205	-.01374
.33271	-.01142
.38555	-.00894
.43995	-.00643
.49528	-.00398
.55088	-.00171
.60605	.00025
.66005	.00182
.71216	.00296
.76168	.00367
.80795	.00397
.85036	.00391
.88834	.00354
.92140	.00295
.94911	.00222
.97109	.00144
.98705	.00073
.99674	.00020
1.00000	-.00000

Fig. 20 S2091-101-83 Coordinates.